第 49 卷 第 19 期/2022 年 10 月/中国激光 特邀综述

中国激光

同步辐射及中子衍射技术在增材制造领域的应用

邓鸿文[1,2,4]，张仪[2,3,4]，权澳冬[1,2,4]，王玉岱[2,3,4]，汤海波[2,3,4]，程序[2,3,4*]

[1]北京航空航天大学材料科学与工程学院，北京 100191；

[2]北京航空航天大学大型金属构件增材制造国家工程实验室，北京 100191；

[3]北京航空航天大学前沿科学技术创新研究院，北京 100191；

[4]大型关键金属构件激光直接制造北京市工程技术研究中心，北京 100191

摘要 近年来，随着“中国制造 2025”的大力推动，增材制造技术已经在航空航天、国防军工等多个战略产业领域展现出了巨大的应用价值和广阔的应用前景，是世界先进制造领域发展最快、技术研究最活跃、关注度最高的研究方向之一。虽然增材制造技术与整体锻造等传统加工方法相比有着诸多优势，但当金属增材制造成形工艺选择不合适时，成形件内部易产生气孔、未熔合等缺陷；同时，制造过程中超快的加热/冷却会在构件中产生较大的残余应力，最终导致构件开裂、变形，显著降低增材制造成形件的内部质量和力学性能。由于增材制造过程涉及十分复杂的材料冶金、物理、化学和热力耦合现象，因此难以通过传统的材料表征手段对其进行分析。随着同步辐射光源和中子源的快速发展，基于同步辐射和中子衍射的表征技术在分析金属增材制造零件内部缺陷和力学性能等方面扮演着越来越重要的角色，这些技术可以阐明增材制造过程中熔池的动力学行为、凝固缺陷的产生机制、构件中应力的分布状态以及非平衡固态相变等过程。本文综述了同步辐射和中子衍射技术在增材制造过程中进行原位观察和应力分析的原理、各自的优势以及它们在增材制造中的实际应用，总结了其应用于金属增材制造技术的最新进展，并对其未来的发展进行了展望。

关键词 激光技术；增材制造；同步辐射；中子衍射；材料表征

中图分类号 TG115.28 **文献标志码** A **DOI**：10.3788/CJL202249.1902002

1 引 言

金属增材制造技术是一种直接制造致密金属零部件的高性能加工成形方法，该技术以金属粉末或金属丝材为原料，用激光、电弧或电子束等高能束按照预设的扫描路径，进行逐点扫描、逐线搭接、逐层熔化和凝固堆积[1]，基于 CAD 模型实现全致密、高性能金属结构件的“近净成形”制造[1-3]。根据所选热源和材料的不同，金属增材制造技术可分为定向能量沉积(DED)技术、电弧送丝增材制造(WAAM)技术以及粉末床熔融(PBF)技术。其中，粉末床熔融技术包括激光选区熔化(SLM)技术、选择性激光烧结(SLS)技术和电子束选区熔化(EBM)技术[4]。与整体锻造等传统加工方法相比，金属增材制造技术具有制造成本低及生产周期短等优势，特别适合制备结构复杂的金属零部件，已成为先进制造技术的前沿研究热点之一，在航空航天及国防军工等战略领域具有重要的应用价值[1-3,5]。

金属增材制造成形过程涉及的热力学条件十分极端，其加热和冷却速率可以达到 10^6 K/s，温度梯度高达 10^3 K/mm[6]。由于在这种极端的热力学条件下进行加工，增材制造过程涉及许多高度动态和瞬态的物理过程，同时存在“激光-粉末/熔池/金属蒸气交互作用”、超高温度梯度和边界条件不断变化下“移动熔池熔体的快速凝固”、三维零件“内部凝固组织和内部缺陷的形成”、复杂约束和非平衡相变条件下零件“内应力的形成和演化”等十分复杂的材料冶金、物理、化学和热力耦合现象[1-2]。同时，伴随着金属增材制造成形过程中能量输入密度、扫描速度和扫描方式的改变，以及熔池中熔体状态的变化等一切不连续和不稳定现象的发生，成形件内部会不可避免地产生各种特有的内部冶金缺陷，例如气孔缺陷、未熔合缺陷以及由残余应力引起的开裂、变形等，这些缺陷会显著影响增材制造成形件的内部质量及力学性能[1-2,7-8]。因此，弄清熔池内部长期周期性热循环过程的动力学行为、理解零件内部缺陷形成的原因、阐明激光成形过程中非平衡循环固态相变机理以及零件内部应力的累积机制，对于提高增材构件的内部质量及力学性能具有重要意义，

收稿日期：2022-07-05；**修回日期**：2022-08-13；**录用日期**：2022-09-13

基金项目：广东省基础与应用基础研究重大项目(2020B0301030001)

通信作者：*chengxu@buaa.edu.cn

而这一直以来都是国内外增材制造领域研究人员关注的重点。然而，金属增材制造成形过程中的熔池小且熔池温度极高，无法采用高速摄像机、扫描电子显微镜(SEM)、X 射线应力分析仪等传统表征手段对熔池内部缺陷的形成以及构件中应力的演变进行实时精准观察及分析，从而使得对构件的成形质量控制较为困难。

近年来，随着同步辐射光源和中子源的快速发展，基于同步辐射和中子衍射的表征技术在增材制造领域被广泛应用[9-11]。同步辐射是相对论性带电粒子在电磁场作用下沿弯转轨道行进时发出的电磁辐射[12]，其波长范围覆盖从近红外线到 X 射线的所有波段，可以用于无损高分辨成像和计算机断层扫描成像等。基于同步辐射的表征技术以其光源的强穿透性、高时空分辨率、高通量等诸多优点，在材料表征方面具有巨大的应用潜力和广阔的科研前景[13]。在增材制造领域，基于同步辐射的表征技术主要被用于激光粉末床熔融(LPBF)和 DED 成形技术中，研究的材料包括钛合金、镍基合金、铝合金等。利用同步辐射 X 射线原位成像技术可以实现原位可视化研究，为分析合金凝固过程、微观组织演变以及金属内部缺陷形成过程的原位观察及分析提供了途径[9-10]；基于同步辐射的计算机断层扫描技术可以精确测量已成形零件的表面缺陷和内部缺陷，且表征分辨率与穿透深度随着光源亮度、探测器灵敏度以及数据处理效率的提高而提高[14]。

中子衍射技术的物理原理与 X 射线、电子衍射相似，皆为 Bragg 方程。当中子流与物质相遇时，由于其本身不带电，不受原子核外电子云的干扰，可以直接与该物质的原子核发生相互作用，因此中子对材料的穿透性更强。相较于测量残余应力的传统方法，如钻孔法、X 射线法、高能同步 X 射线法等[7]，中子衍射法在表征残余应力方面具有显著优势[15]，其探测的样品厚度可以达到厘米级别。中子流与物质的原子核作用后会产生各向同性的散射，散射振幅与待测元素的原子序数无关，只随原子磁矩的大小和取向而改变，因此，中子衍射技术可以准确地辨别出待测样品的元素组成，从而可以鉴定元素组成相似的材料[16]。此外，与同步辐射等衍射技术一样，中子衍射也可以原位无损地研究材料制备和加载过程中的力学行为和晶粒取向等。利用当下最先进的散裂中子源及分析技术[17]可以在超高温/低温、应力等复杂外场环境下进行原位中子衍射实验，分析材料的晶粒旋转、多尺度应力配分、相变与孪晶作用机制等[18]。在增材制造领域，中子衍射技术除了能够研究构件的内部宏观残余应力以外，还能够无损高分辨地测量金属构件内部的晶相、应变、晶粒尺寸、位错和织构等晶体结构信息在实空间中的二维甚至是三维分布，也可以分辨出氢、锂等轻元素的数量以及它们在结构中的确切位置。与同步辐射技术相比，中子衍射技术还可以获得精度更高的点阵应变，从而可以对金属材料中的织构和残余应力进行更深入的研究。此外，基于飞行时间(TOF)技术的中子反射谱仪(TPNR)在多尺度下的材料内部应力测量与组织研究方面更具优势，它还可以进行微观力学和相变模型的验证[19]。

将基于中子衍射和同步辐射的表征技术协同配合，可以对材料进行原位高分辨分析，弄清增材制造成形件服役期间的微观结构变化与应力应变演化规律，为提高增材构件的内部质量和力学性能提供可靠途径。中子衍射和同步辐射技术在材料科学和工程领域具有巨大的应用潜力。本文综述了同步辐射和中子衍射技术在增材制造过程中进行原位观察和应力分析的原理、各自的优势及其在增材制造中的应用实例，总结了其应用于金属增材制造技术的最新研究进展，并对其未来的发展进行了展望。

2 同步辐射及中子衍射技术在增材制造领域的应用

基于中子衍射和同步辐射的表征技术在增材制造领域中的应用主要包括 4 个方面：1)原位观察金属增材制造成形过程中的熔池动力学行为以及内部缺陷的形成过程；2)原位观察零件内部缺陷在原位拉伸/疲劳试验过程中对增材构件的影响；3)原位检测增材制造过程中内应力的累积和测量成形零件的残余应力；4)检测增材制造过程中的相变动力学行为以及实时分析微观织构的演化。基于同步辐射和中子衍射的表征技术研究的增材制造工艺、材料等如表 1、表 2 所示。

表 1 基于同步辐射的表征方法在增材制造中的应用

Table 1 Application of characterization methods based on synchrotron radiation (SR) in additive manufacturing

Technique	Facility	Beamline	Material	Method	Study field
LPBF	European Synchrotron Radiation Facility (ESRF)	ID19 ID-31	Ti6Al4V[20-22] Inconel 625[23]	Imaging SR-XRD μ-CT	Melt pool dynamics[21] Powder dynamics[20-21] Pore evolution[20] Phase transformation[22] Surface defects[23]

（续表）

Technique	Facility	Beamline	Material	Method	Study field
LPBF	Diamond Light Source	I12-JEEP	Invar 316L[24-26]	Imaging	Melt pool dynamics[24-26] Powder dynamics[24-26] Pore evolution[24-26]
DED	Diamond Light Source	I12-JEEP	SS316[27] Ti6Al2Sn4Zr2Mo[27] Inconel 718[28]	Imaging SR-XRD	Melt pool dynamics[27-29] Pore evolution[27] Phase transformation[28] Stress evolution[28] Micro-cracks evolution[28]
LPBF	Advanced Photon Source (APS)	32-ID-B 35-ID 2-BM	Ti6Al4V[6,30-45] Al6061[31,37,46-49] Al10SiMg[30,34,40-42,48-51] 17-4 PH SS[52] 316L[50,53] AISI 4140 Inconel 718[30,54] SS316[46,54] Al alloys[55] Ti10V2Fe3Al[56]	Imaging SR-XRD Dynamic X-ray radiography	Melt pool dynamics[6,30,32-33,35-41,43-44,46-49,51,53,56] Powder dynamics[6,30,32,34-37,40,42-43,47,49,50,52] Pore evolution[6,31,33-35,37-41,46-47,49,52] Phase transformation[6,34,44,54,56] Cracks evolution[54-55] Surface defect[45]
DED	Advanced Photon Source (APS)	32-ID-B	Ti6Al4V[57-59] MoNbTiV[60] CoCrFeMnNi[61]	Imaging	Powder dynamics[57] Melt pool dynamics[58-60] Pore evolution[58-60] Mixing of high entropy alloys during laser remelting[61]
LPBF	Deutsches Elektronen Synchrotron (DESY) PETRA Ⅲ	HEMS-beamline P07	CMSX-4[62-63] Inconel 625[63-65] γ-TiAl[63] Pure Ti[66]	WAXS SAXS SR-XRD	Phase transformation[62-63,66] Stress evolution[63-66] Lattice spacing[63,65]
DED	Deutsches Elektronen Synchrotron (DESY) PETRA Ⅲ	HEMS-beamline P07	X40CrMoV5-1 steel[67]	SR-XRD	Microstructural evolution[67] Lattice parameter evolution of γ-Fe[67]
LPBF	Stanford Synchrotron Radiation Laboratory (SSRL)	2-2 10-2	Ti6Al4V[68-73] Ti5Al5V5Mo3Cr[74] SS316L[70,72] Al6061[71] Ni400[71]	Imaging SR-XRD	Melt pool dynamics[68,70,72-74] Pore evolution[68,70-74] Lattice dynamics[68-69] Phase transformation[68-69,74] Stress evolution[69]
LPBF	Swiss Light Source (SLS)	MicroXAS & MS TOMCAT	Ti6Al4V[75-76] CM247LC[77] AlSc(Zr)[78]	Imaging SR-XRD	Phase transformation[75-76,78] Stress evolution[76] Cracks evolution[77]
DED	Cornell High Energy Synchrotron Source	ID3A	Inconel 625[79] SS304[79]	Imaging SR-XRD	Lattice strain[79]

表 2 基于中子衍射的表征方法在增材制造中的部分应用

Table 2 Partial application of characterization methods based on neutron diffraction in additive manufacturing

Technique	Facility	Material	Detector	Study field
LPBF	J-PARC	AlSi3.5Mg2.5[80]	TAKUMI	Explore evolution of phase stresses, dislocation density, and crystallite size[80]
LPBF	Oak Ridge National Laboratory (ORNL)	Inconel 625[81] 304L stainless steel[82]	VULCAN engineering materials diffractometer[81-82] Time-of-flight neutron diffraction instrument[81]	Measures residual stresses[81] Characterizes crystallographic texture[82]
LPBF	The Australian Nuclear Science and Technology Organization (ANSTO)	Inconel 718[83]	KOWARI engineering diffractometer	Measures residual stresses[83] Visualize and quantify the distribution of internal defects and macro-porosities[83]
LPBF	ISIS	316L stainless steel[84]	ENGIN-X	Revealed mechanical and microstructural responses[84]
LPBF	NIST's CNR	Stainless steel 17-4 PH[85]	BT8 residual stress diffractometer Ordela 1150 position sensitive neutron detector	Measures internal residual stresses Measures lattice strains[85]
LPBF	The Australian Nuclear Science and Technology Organization (ANSTO)	Ti-6Al-4V[86]	KOWARI-strain scanner	Measures residual stresses[86]
LPBF	Helmholtz-Zentrum für Materialien und Energie, Berlin (HZB)	Inconel 718[87]	2D detector	Measures residual stresses[87]
Cold spray additive manufacturing (CSAM)	ANSTO	Ti/Fe coated sample[88]	KOWARI	Measures residual stresses[88]
WAAM	ANSTO	TiAl[89]	KOWARI	Measures residual stresses[89]
WAAM	ISIS	Inconel 718[90]	GEM	Measures texture[90]
WAAM	ISIS	Ti-6Al-4V[91]	ENGIN_X	Measures residual stresses[91]
DED	J-PARC	CoCrNi[92]	TAKUMI	Measures lattice strain[92]
DED	Oak Ridge National Laboratory (ORNL)	Inconel 625[93-95]	VULCAN engineering materials diffractometer	Measures residual stresses[93-94] Characterizes crystallographic texture[95]
DED	ISIS	Nickel-base super alloy C263[96]	ENGIN_X	Measures residual elastic strain and crystallographic[96]
EBM	Oak Ridge National Laboratory (ORNL)	Inconel 718[97-98]	VULCAN engineering materials diffractometer	Measures crystallographic texture[98] Measures peak positions of individual planes and lattice strains[97]

（续表）

Technique	Facility	Material	Detector	Study field
EBM	National Institute of Standards and Technology (NIST)	Ti-6Al-4V[99]	BT8 residual stress diffractometer	Measures residual stresses[99]
EBM	Canadian Neutron Beam Center	Ti-6Al-4V[100]	L3 diffractometer	Measures thermal residual stress[100]
Direct metal laser sintering (DMLS)	Los Alamos Neutron Science Center (LANSCE)	GP1 stainless steel[101]	HIPPO instrument	Measures texture[101]
Direct metal laser sintering (DMLS)	Canadian Nuclear Laboratories	316L stainless steel[102]	L3 diffractometer	Measures residual stresses[102]

2.1 原位检测熔池动力学行为及其内部缺陷演化过程

众所周知，在金属增材制造成形过程中，激光-粉末/熔池/金属蒸气之间复杂的交互作用会导致成形件内部产生或重熔冶金缺陷[58-60]，且熔池内部熔体的流动和导热模式改变会导致熔池内部缺陷位置发生改变，从而影响熔池内部缺陷的演化过程[21,24-26]。借助同步辐射 X 射线成像技术可以原位观察极端热力学条件下入射高能束与金属粉末之间的交互作用，分析其对熔池内部缺陷演化过程的影响。研究结果表明，激光-粉末/熔池/金属蒸气之间复杂的交互作用会直接影响增材制造成形过程中的熔池深度[33]、小孔的形成和演变[26,37-38]、元素的蒸发[53]以及金属熔体的流动速度和方向[72,103]，过高的能量输入还会直接导致金属液滴或者熔池附近未熔化的粉末颗粒飞溅[30,104]，从而使成形件内部产生冶金缺陷[42]并影响成形件的表面粗糙度[21]。Young 等[42]研究了 LPBF 成形过程中激光-粉末之间的交互作用导致的金属粉末/熔体飞溅过程，并对各类飞溅物的形成机理和特征进行了定性和定量分析；结果显示：LPBF 工艺中的工艺参数（激光功率、扫描速度和环境压力）直接决定成形过程中的飞溅类型及其特征，从而影响成形件内部孔隙及缺陷的分布。通过建立合适的物理模型，可以模拟激光扫描过程中金属熔体和粉末的运动状态[29]；通过同步辐射 X 射线成像技术对模拟结果进行验证，可以更深入地了解激光成形过程中的粉末动力学行为与内部缺陷之间的关系[57]。Jakumeit 等[104]将简单拉格朗日模型的粒子加速模型进行扩展，使用 Eulerian 多相方法对 LPBF 工艺中金属粉末的熔化、蒸发和凝固过程进行模拟，以分析激光扫过时的粒子飞溅；然后通过同步加速器 X 射线成像测试分析了 Ti-6Al-4V 增材制造过程中的粒子飞溅动力学，并将测试结果与模拟结果进行了比较。

同步辐射 X 射线成像技术还可以用于原位分析增材制造过程中的熔池动力学行为。研究结果表明，熔体的流动模式会直接影响熔池的几何形态，而熔池的几何形态及其在增材制造成形过程中的演变过程与成形件的微观结构及内部缺陷的形成直接相关[20,32,51]，从而影响增材制造成形件的力学性能[21,25]。Leung 等[25]使用英国钻石光源（Diamond Light Source）公司的 I12-JEEP 光束线进行原位同步 X 射线成像，观察了 LPBF 过程中内部缺陷形成的过程，揭示了由 Marangoni 对流引起的熔池内部孔隙迁移与形成过程。如图 1 所示，大多数孔隙在 Marangoni 对流作用下沿液固界面前沿向外向下移动，之后在浮力作用下于熔池的中间部位上升；金属凝固结束后，靠近顶部的部分孔隙会破裂，其中气体逸出，从而在成形件内部留下气孔缺陷。通过建立增材制造工艺参数与熔池动力学之间的关系[103,105-106]，研究人员模拟了增材制造成形过程中熔池几何形态的演化过程[29,33,48]，熔池几何形态的演化对于控制增材制造成形件的力学性能至关重要。Guo 等[48]采用基于同步辐射的原位高分辨率同步 X 射线成像技术，记录了不同工艺参数下增材制造过程中的熔池行为，首次揭示和量化了不同传热模式下熔体在熔池不同区域的流动模式，分析了不同类型熔体流动的驱动力，阐明了熔体在熔池不同位置处的动能衰减和导热模式。

随着同步辐射 X 射线成像技术在原位观察激光熔化沉积成形构件内部冶金缺陷的形成以及熔池、粉末动力学方面的研究成果越来越多，研究人员开始根据目前已知的机制对增材制造零件的性能进行一定的调控。例如，Qu 等[47]使用基于 APS 光源的 X 射线成像技术研究了 Al6061 成形过程中激光与粉末层的交互作用，并通过向 Al6061 粉末中添加

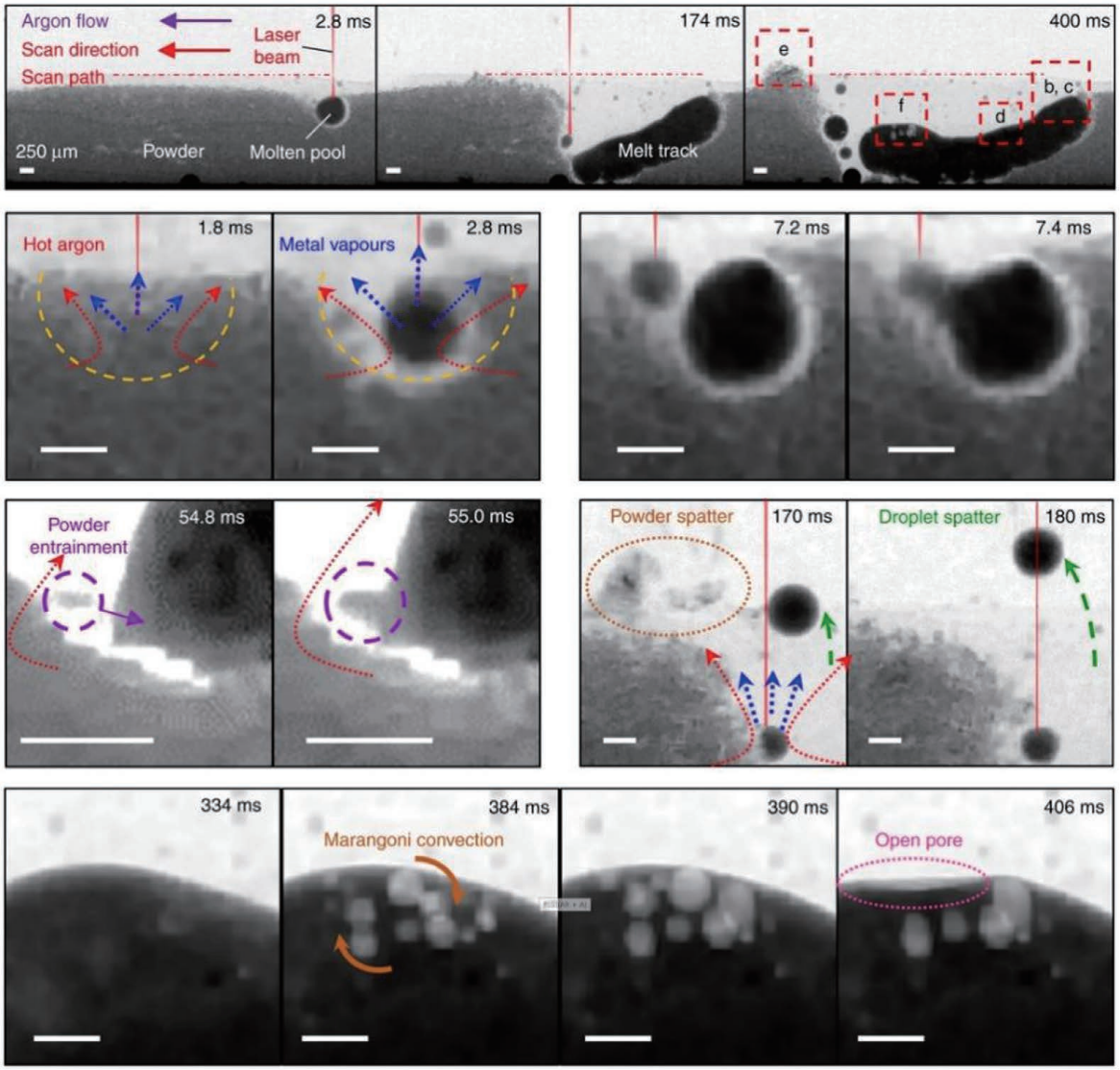

图 1 在激光扫描过程中，单层 Invar 36 粉末熔道轨迹随时间变化的照片，照片捕捉了反冲压力在激光扫描过程中对金属粉末运动的影响以及孔隙在 Marangoni 对流作用下的运动轨迹[25]

Fig. 1 Time-series radiographs acquired during laser additive manufacturing (LAM) of Invar 36 single layer melt track. The effect of recoil pressure on metal powder movement and trajectory of pores under Marangoni convection were discovered[25]

TiC 纳米颗粒来控制激光与粉末床相互作用过程中的不稳定性，消除了大型粉末的溅射，如图 2 所示。这一方法使得零件的内部缺陷减少，零件内部的均匀性变好，零件的性能得以提升。Hojjatzadeh 等[40]使用基于 APS 光源的高速硬 X 射线成像技术揭示了 LPBF 过程中熔池中微孔的高度动态和复杂运动。他们将复杂的原位实验和多物理建模相结合，揭示了孔隙移动行为与温度梯度引起的热毛细力、熔体流动引起的阻力有关。他们发现激光相互作用区域的温度梯度所产生的高热毛细力可以克服熔体流动产生的阻力，从而快速消除熔池中的气孔，由此提出了一种有效消除金属 3D 打印件孔隙的机制，并基于该机制实现了极低孔隙率增材制造零件的成形。

2.2 原位分析内部缺陷对增材构件力学性能的影响

在增材制造成形件服役过程中，孔隙的萌生和聚集是增材构件中裂纹形成的主要机制[107]。高孔隙率的成形件往往力学性能相对较差[108]。研究人员已经通过对增材构件内部孔隙的尺寸、体积分数和空间分布等进行了研究[109]，并发现可以通过在一定范围内增加电子束的能量密度来降低增材构件内部的孔隙率[110-111]。基于同步辐射的计算机扫描技术可以应用于原位拉伸试验中实时监测成形件内部缺陷对疲劳损伤积累和裂纹扩展的影响。例如，Wu 等[112]在欧洲同步辐射光源(ESRF)和斯坦福同步辐射实验室(SSRL)对 7020-T65 合金激光复合焊接头进行了标准疲劳测试和原位疲劳测试，并基于传统有限元法和新发展的杂交多边形有限单元法(HPE)阐释了孔隙和裂纹在应力集中因子、应力强度因子方面的相互作用，揭示了孔隙分布在裂纹尖端的应力场中所起到的作用。孔隙的存在会使短裂纹的传播变得复杂，其在裂纹稳定生

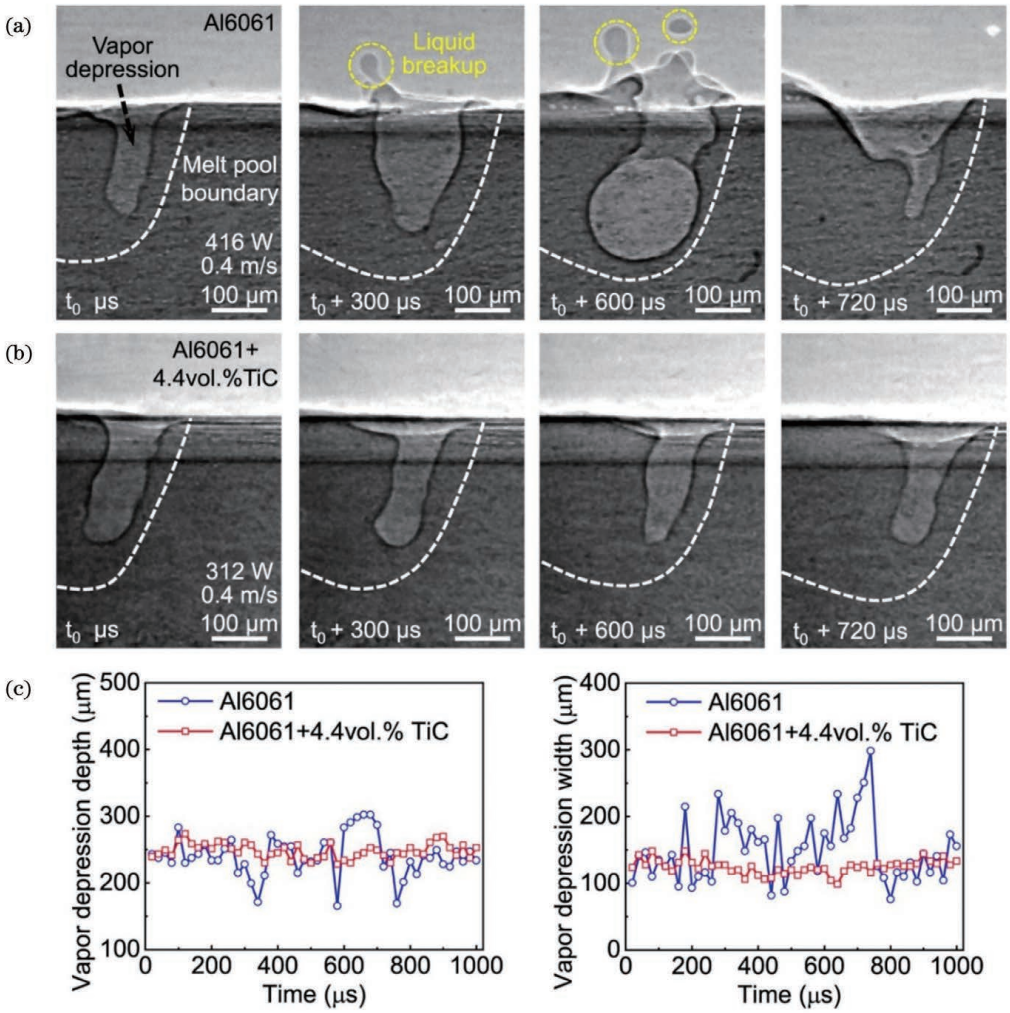

图 2 金属增材制造过程中的不稳定性控制[47]。(a)X 射线图像捕获了 Al6061 激光熔化过程中的液体破裂过程，破碎的液泡用虚线圆圈表示；(b) Al6061+4.4%TiC 熔化过程中的 X 射线图像，液体内的气压更稳定，液体不会破裂；(c)激光熔化过程中蒸气压深度和宽度随时间的变化

Fig. 2 Controlling instability during metal additive manufacturing[47]. (a) X-ray images showing liquid breakup during laser melting of Al6061, where the broken liquid is indicated by dashed circle; (b) X-ray images showing laser melting of Al6061+4.4% TiC, the pressure in liquid is stable and the liquid will not break; (c) vapor depression depth and width evolution with time during laser melting

长阶段对裂纹生长的影响较小，但在裂纹断裂临界点处，会使疲劳裂纹增长率发生明显波动。如果在裂纹扩展路径上存在较大的孔隙，裂纹的预期生长路径就会发生改变。Bao 等[113]使用延时同步辐射 X 射线显微计算机断层扫描技术(SR-μCT)，观察了 SLM 成形 AlSi10Mg 构件在循环载荷下的高温(250 ℃)拉伸试验中的疲劳损伤积累，并将其与室温拉伸试验中构件的疲劳损伤积累进行了对比，揭示了高应力比低周疲劳条件下，缺陷对 AlSi10Mg 合金高温疲劳损伤积累的影响，如图 3 所示。

研究人员也建立了一些理想的力学模型，用来预估增材构件的疲劳寿命和服役寿命，并通过基于同步辐射的原位测试进行了验证，以便更好地了解内部缺陷几何特征与成形件性能之间的关系。Hu 等[114]提出了一种基于贝叶斯框架修正的概率损伤演化模型，并将采用同步辐射计算机断层扫描技术重建的 SLM 成形 Ti-6Al-4V 样品的初始孔隙形态作为损伤演化模型的输入，最终通过基于同步辐射 X 射线断层扫描技术的原位单轴拉伸试验和标准棒单轴拉伸试验验证了该模型的预测能力。Qian 等[115]进行了原位拉伸试验，研究了 SLM 成形 AlSi10Mg 合金在高周疲劳下由未熔合缺陷引起的疲劳损伤和失效行为；他们还借助同步辐射 X 射线断层扫描技术测量了多个缺陷，建立了多重疲劳裂纹扩展模型，以描述多裂纹之间的协同效应以及评估材料的疲劳寿命。

2.3 增材制造成形过程中内应力的累积机制及残余应力的测量

宏观上，零件内部残余应力的来源可以通过 Mercelis 等[116]提出的临界温度梯度机制(TGM)解释，但目前还没有一套确切的理论能解释复杂热力学条件下激光长期熔化沉积过程中的内应力累积机制。同步辐射 X 射线衍射技术和中子衍射技术可以通过

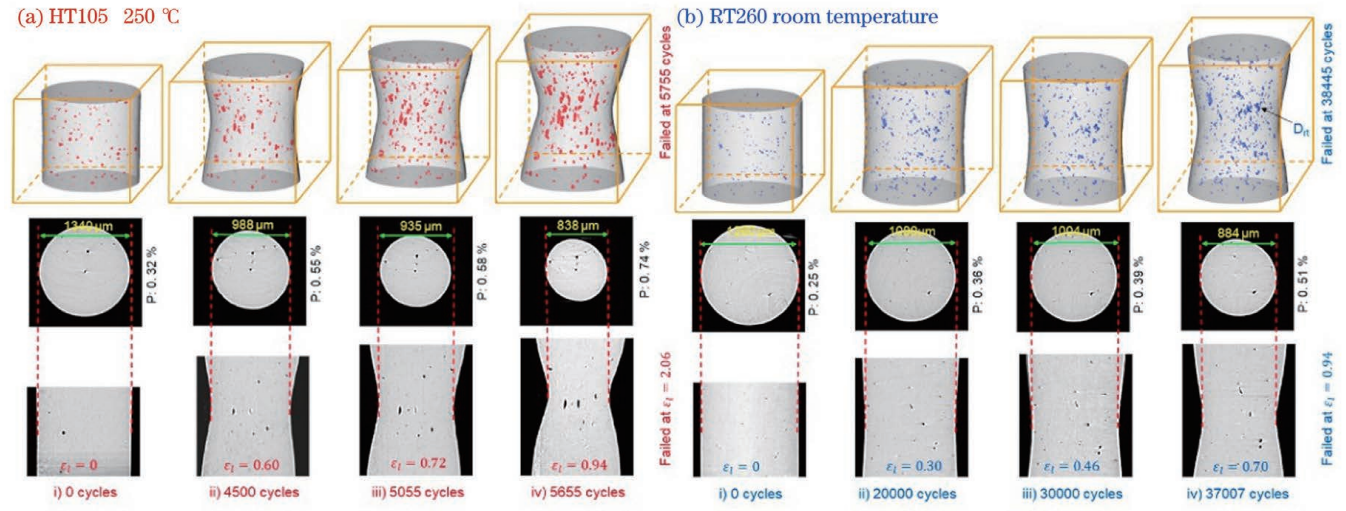

图 3 不同循环次数下样品的延时图像[113]，第一行是孔隙的三维图像，第二行是模拟颈缩处切片的三维图像，第三行是纵向切面的三维图像。(a) 在 250 ℃和 105 MPa 峰值载荷下测试的 AlSi10Mg 样品(HT105)；(b)在室温和 260 MPa 峰值载荷下测试的 AlSi10Mg 样品(RT260)

Fig. 3 Time-lapse images of samples at different numbers of cycles[113], where the first, second, and third rows show three-dimensional images of voids, virtual slice at neckdown position, and longitudinal section. (a) AlSi10Mg sample (HT105) tested at 250 ℃ and peak load of 105 MPa; (b) AlSi10Mg sample (RT260) tested at room temperature and peak load of 260 MPa

原位采集衍射花样进行实时数据分析，获得增材构件中内应力的分布状态[64,66]。现有研究结果表明，增材制造成形过程中的温度梯度和冷却速率可以直接影响成形零件中的残余应力水平[28,69]，不同的扫描策略也会对成形件中的残余应力分布产生影响[76]。如图 4 所示，Serrano-Munoz 等[117]使用同步加速器 X 射线能量色散衍射(EDXRD)与光学轮廓测量相结合的方法，研究了三种不同扫描策略(Y 扫描、90° *XY* 扫描和 67° 旋转扫描)下，LPBF 成形 Inconel 718 合金在基板移除时的残余应力分布状态和微观结构变形。Schmeiser 等[64]利用 DESY 的 P07 HEMS 光束线对 Inconel 625 的 SLM 成形过程进行原位衍射实验，观察到了单层中的横向热量积累以及成形方向上的垂直热量积累，解释了激光-金属相互作用过程中与应力相关的一些

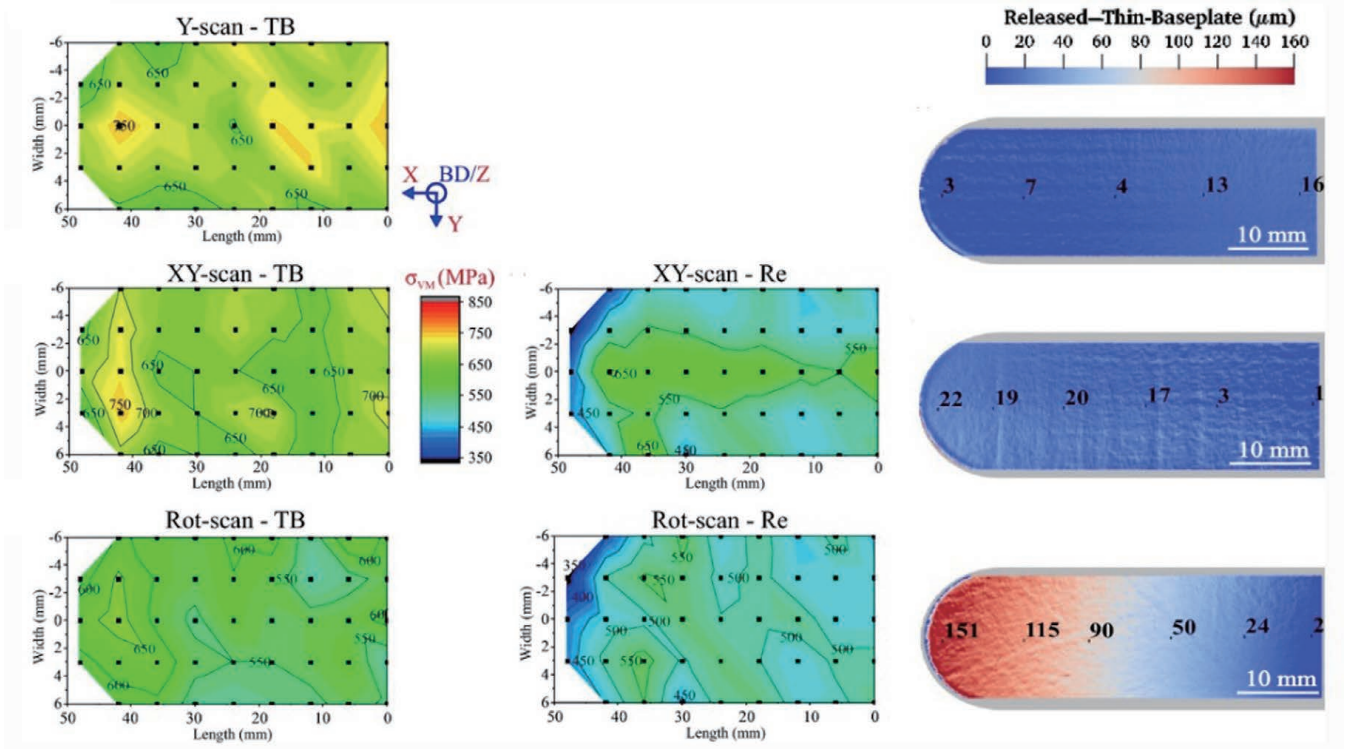

图 4 薄基板条件下样品顶部的 Von Mises 残余应力图[117]

Fig. 4 Von Mises residual stress (RS) at the top of sample in thin-baseplate (TB) condition[117]

现象。Schmeiser 等[66]使用同步辐射 X 射线衍射方法研究了商业纯钛零件在 LPBF 过程中的亚表面相变和内应力形成过程。

除了研究增材制造过程中内应力的累积机制以外，受益于同步辐射和中子流的优异特性，基于同步辐射和中子衍射的应力表征技术在构件内部残余应力的测量方面也具有显著优势。研究人员不仅基于同步辐射和中子衍射的应力表征技术测量了金属大型结构件内部的残余应力[118-120]，还基于所测得的残余应力数据建立了合适的力学模型[63,65]，并通过原位拉伸试验对所建模型进行了验证[88]。Shen 等[89]在实验中使用的 KOWARI 装置是常用的残余应力测量设备，实验中测量点的分布和设备示意图如图 5(a)、(b)所示。基于中子衍射技术测量零件晶格畸变的实验装置如图 5(c)所示，Kim 等[92]采用中子衍射技术测量了 DED 成形 CoCrNi 中熵合金(沉积态)中严重的晶格畸变。Aminforoughi 等[121]使用基于 LPBF 加工的具有复杂微观结构的 Inconel 718 合金以及常规制造的 100Cr6 钢样品进行原位拉伸模拟试验，验证了一种基于线性回归的残余应力评估新方法——$\sin^2\alpha$ 方法，该方法可以精确地分析增材制造构件内部不同位置的残余应力。

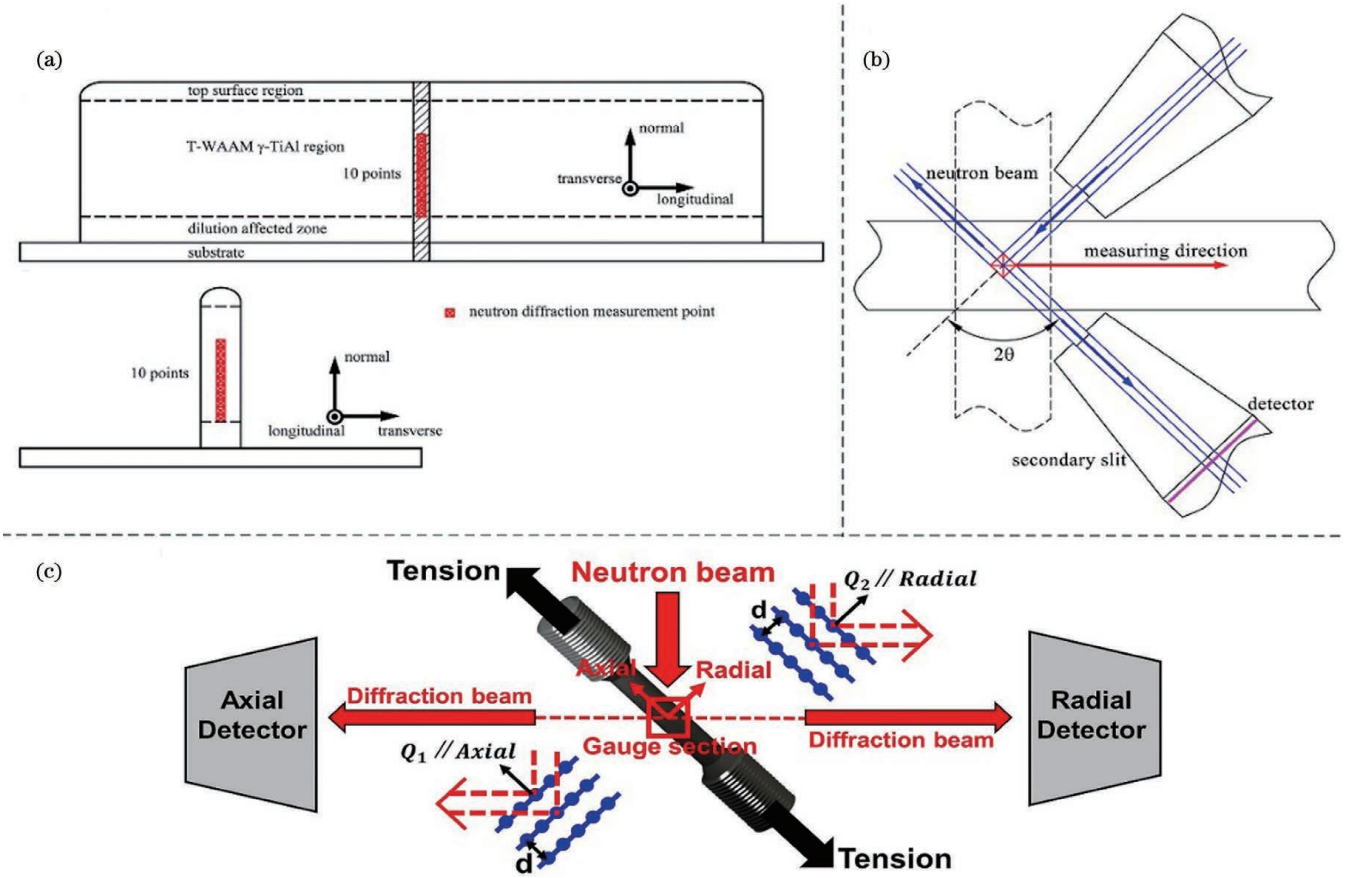

图 5 增材制造金属构件的残余应力测量。(a) 中子衍射残余应力测量样品上测量点的分布[89]；(b) 实验中用于残余应力测量的 KOWARI 中子衍射装置示意图[89]；(c) 测量晶格应变的原位中子衍射实验示意图[92]

Fig. 5 Measurement of residual stress in metal components prepared by additive manufacturing. (a) Distribution of measurement points on the sample for neutron diffraction residual stress measurement[89]; (b) schematic of KOWARI neutron diffraction device for residual stress measurement in experiment[89]; (c) schematic of *in-situ* neutron diffraction experiment for measuring lattice strain[92]

2.4 增材制造成形过程中相变动力学行为及微观织构的演化

目前，研究人员已经对增材制造中的固态相变过程进行了广泛而深入的研究[122]，并建立了时间-温度-转变(TTT)图，但当前的研究主要集中于非原位分析增材制造过程中的固态相变，很难实时检测增材制造过程中的短时非平衡固态相变[25]。基于同步辐射的众多优异特性，同步辐射 X 射线衍射技术可以原位检测增材制造过程中的非平衡固态相变[68-69,74]，这对于了解增材制造过程中的复杂动力学机制有很大帮助，而且与非原位实验相比，原位实验在研究金属材料可逆弹性变形机制方面更具优势[123-124]。Wahlmann 等[125]使用基于同步辐射的小角 X 射线散射(SAXS)对电子束选区熔化(SEBM)成形的镍基高温合金 CMSX-4 中的 γ′相进行表征，研究了循环加热和淬火期间 γ′相的析出和溶解，分析了 γ′相在增材制造过程中的析出过程和动力学模型，如图 6(a)所示。Beese 等[126]利用 VULCAN 装置进行原位中子衍射表征，将

得到的晶格应变数据与其所提出的位错阻滞模型相结合解释了动态应变时效(DSA)在镍基合金中消失的原因。Mori 等[127]采用中子衍射技术对电子束粉末熔融制备的 Ti-6Al-4V 进行了表征,他们选择高强度中子源,成功分析出了先析出 β 相、α 板条和纳米级 β 相之间的多重取向关系。Sofras 等[82]研究了 304L 不锈钢塑性与宏观结构的相关性,并获得了一系列原位中子衍射实验数据,实验数据显示了拉伸试样中马氏体的体积分数随应变的演变,如图 6(b)所示。Xie 等[128]利用原位中子衍射研究了铸态锆合金在热循环期间的相变过程,结果显示,加热和冷却会显著改变锆合金的晶格参数、原子有序程度和晶胞体积等。Tang 等[84]利用原位中子衍射技术研究了 LPBF 制备的 316L 奥氏体不锈钢(ASS)在拉伸过程中的变形机制,并证实了应变诱发孪晶转变是马氏体形成的主要变形机制。Clausen 等[101]在研究增材制造 GP1 不锈钢的相变行为时,于热处理和单轴加载期间进行了原位中子衍射测量,结果发现了显著的奥氏体到马氏体相变,并且材料的强化随着马氏体体积分数的增加而增大。

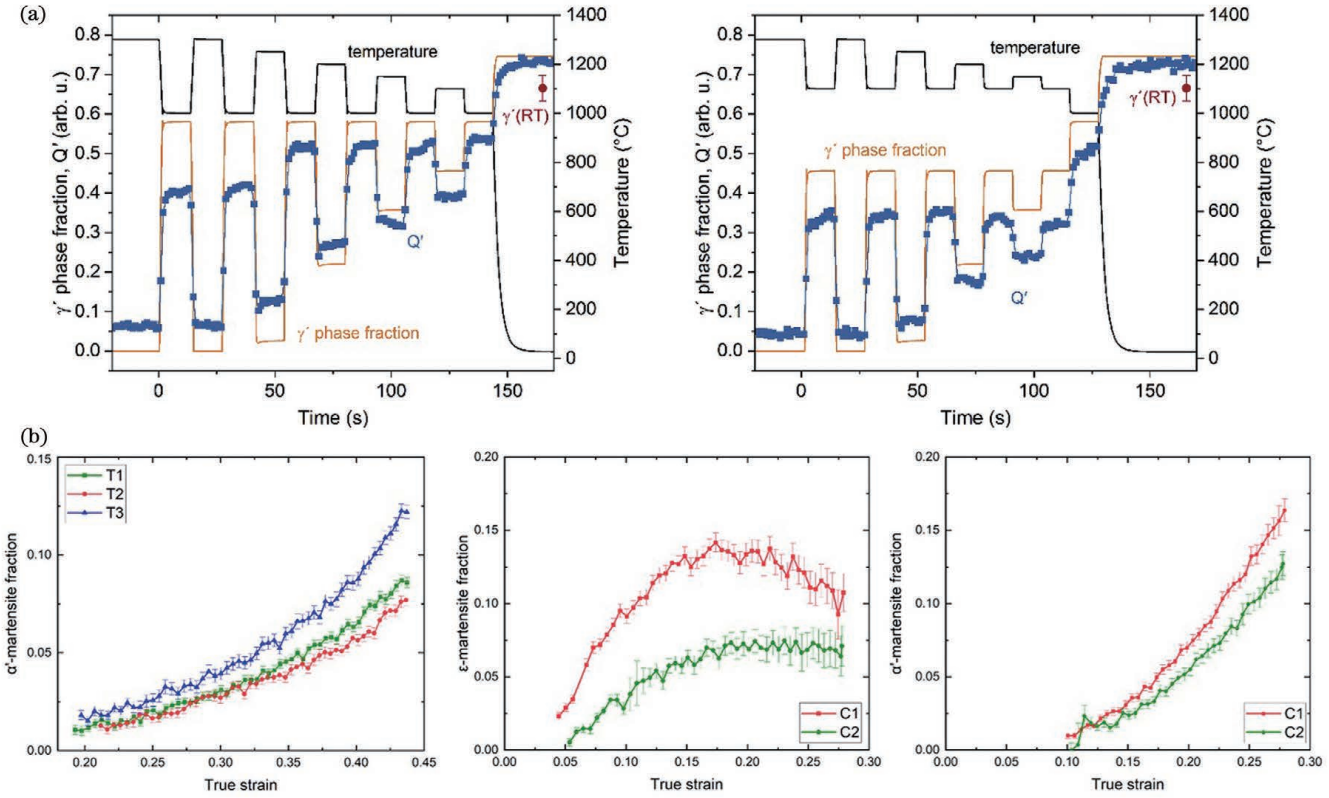

图 6 增材制造金属构件的固态相变演变及分析。(a)测量和计算得到的 γ′相在热循环过程中的体积分数演变图[125];(b)拉伸试样中马氏体体积分数与真应变的关系[82]

Fig. 6 Evolution and analysis of solid-state phase transformation of additive manufacturing metal components. (a) Evolution of measured and calculated volume fraction of γ′ phase during thermal cycling[125]; (b) relationship between martensite phase volume fraction of tensile sample and true strain[82]

除了测量增材制造成形过程中的固态相变过程以外,基于同步辐射和中子衍射的表征技术还可以对增材制造成形过程中微观结构的变化进行分析。此外,基于同步辐射和中子衍射的原位实验不仅能够探究增材制造成形件在载荷影响下的晶体织构[63,65]、晶格畸变的特性[68-69],还能够在相变过程中测量位错密度和位错柏氏矢量组成[129-130]。在微观层面上看,基于中子衍射的表征技术比基于同步辐射的表征技术所能测得的有效体积更大,即便是在数十微米的体积内也能较好地统计、测量织构和晶格应变,并且通过观察和分析衍射峰的位移、宽化和不对称性,可以进一步得到孪生层错概率、位错密度、堆垛层错能[80]。高钰璧等[131]利用原位中子衍射室温压缩等实验,结合 Ashby[132]提出的位错演化模型,得到如下结论:随着变形速率增加,合金的总位错密度先减小后增加,其中的几何必须位错密度单调递增,统计存储位错密度单调递减。Laquai 等[133]采用同步辐射折射和透射技术(SXRR),研究了 SLM 成形的 Inconel 718 合金分别处于沉积态、无热等静压处理直接时效态、热等静压处理后两步时效态时,微观结构所表现出的不连续性。Miao 等[129]在室温下对超声增材制造的锆进行原位单轴拉伸试验,利用广角 X 射线散射(WAXS)扫描揭示了拉伸过程中整个区域的微观结构变化,并测量了三个代表性轴向位置处位错总密度随真应变的变化,如图 7 所示。Li 等[134]将 4 种通过 LPBF 制得的 Ni-Cr-Si 合金在 1600~11000 K/s 的冷却速率下快速冷却,然后采用

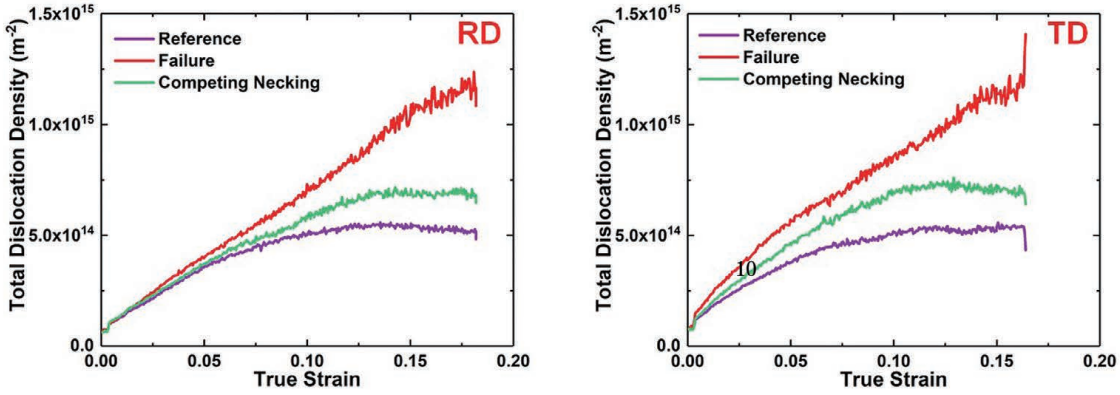

图 7 三个代表性轴向位置处位错总密度随真应变的演化[129](RD:平行于声极滚动方向;TD:平行于声极振动方向)

Fig. 7 Evolution of total dislocation density at three representative axial positions versus true strain[129] (RD: parallel to sonotrode rolling direction; TD: parallel to sonotrode vibration direction)

同步辐射 X 射线微束衍射法对凝固后的微观结构进行原位表征,同时使用扫描电子显微镜(SEM)和 X 射线衍射仪(XRD)进行非原位表征,研究了冷却速率和化学成分对 Ni-Cr-Si 合金微观结构形成和潜在相变机制的影响。

中子不带电并且不具有破坏性,这使得中子衍射技术在增材制造的生物材料研究中也被广泛应用。中子作为核散射,其散射长度不会随原子序数的变化而改变,因此,在轻元素以及原子序数相近的元素检测中,中子衍射技术不可替代。魏志勇等[135]通过测量散射中子的强度函数得到了生物大分子的体积、质量、形状、回转半径,同时还得到了生物大分子中的原子成分、特定原子所处的位置及其分布、生物大分子的动力学信息等。此外,他们使用中子衍射技术对氢元素进行测量,得到了生物大分子中氢的位置、空间分布及其运动行为等信息。中子衍射技术具有超高的穿透力,衍射区域的化学成分、材料的宏观内应力和测试温度都会使对应的峰位发生一定程度的偏移,并产生晶面间距的相对变化。材料中相的体积分数不同,对应的峰的强度也不相同。晶粒尺寸与微观应力也会对峰的形状产生一定影响[136]。正因为如此,中子衍射技术在增材制造金属材料的四维表征上具有广阔的应用前景。随着先进材料和先进技术的不断发展,中子衍射技术的应用不断拓展,其在增材制造领域将成为不可替代的检测技术。

3 结束语

近年来,随着基于同步辐射和中子衍射的表征技术越来越多地被应用于增材制造领域,研究人员在金属内部缺陷形成机理、缺陷致疲劳损伤失效过程追踪,以及增材制造成形过程中熔池的动力学行为、内应力累积和非平衡固态相变等研究方向均取得了一系列成果。随着 2025 年北京怀柔第四代同步辐射光源的建成与投入使用,基于同步辐射和中子衍射技术的表征技术无疑会在增材制造领域扮演着更加重要的角色,帮助研究人员解决增材制造中长期存在的“瓶颈问题”。虽然基于同步辐射和中子衍射的表征技术为深入了解增材制造的成形机制提供了可靠途径,但目前该技术在增材制造领域的应用仍然不够成熟,需要进一步研究,以扩大其在增材制造成形过程中的应用。该技术未来的发展方向如下:

1) 目前,基于同步辐射和中子衍射的表征技术的相关原位检测试验还不够完善,需将增材制造成形过程中的熔池温度场、冷却速率、凝固参数等影响成形件质量的重要因素与打印件的实时模型相结合,以控制成形件的内部质量,提高零件的性能。基于更高光强的同步辐射和中子源所发展的多种先进材料表征方法,需要结合高分辨和高速 X 射线成像技术,因此亟需发展更高时空分辨率与衬度敏感性的原位表征技术,以揭示增材制造成形件内部缺陷的产生机制以及建立可靠的熔池动力学模型,进而指导增材制造工艺参数的设计与优化。

2) 以增材制造成形的关键零部件为例,利用基于同步辐射和中子衍射的 X 射线衍射和应力分析技术,进行金属增材制造成形过程和金属服役过程中应力分布状态以及微观组织演化的表征,建立增材制造成形过程中应变和相变机制的动力学模型,并使用非原位方法进行模拟验证。

3) 中子衍射技术的三维测量优势使其能对增材制造构件裂纹尖端的应力场分布进行监测与观察,从而建立成形件的弹塑性非线性微观力学模型,揭示由复杂多尺度应力场变化导致的各种疲劳、断裂机制。

参 考 文 献

[1] 王华明. 高性能大型金属构件激光增材制造:若干材料基础问题[J]. 航空学报, 2014, 35(10): 2690-2698.
Wang H M. Materials' fundamental issues of laser additive manufacturing for high-performance large metallic components [J]. Acta Aeronautica et Astronautica Sinica, 2014, 35(10): 2690-2698.

[2] 王华明, 张述泉, 王向明. 大型钛合金结构件激光直接制造的进展与挑战(邀请论文)[J]. 中国激光, 2009, 36(12): 3204-3209.
Wang H M, Zhang S Q, Wang X M. Progress and challenges

of laser direct manufacturing of large titanium structural components (invited paper)[J]. Chinese Journal of Lasers, 2009, 36(12): 3204-3209.

[3] 汤海波, 吴宇, 张述泉, 等. 高性能大型金属构件激光增材制造技术研究现状与发展趋势[J]. 精密成形工程, 2019, 11(4): 58-63.
Tang H B, Wu Y, Zhang S Q, et al. Research status and development trend of high performance large metallic components by laser additive manufacturing technique[J]. Journal of Netshape Forming Engineering, 2019, 11(4): 58-63.

[4] 于忠斌, 张中标, 尹婷婷, 等. 金属 3D 打印技术概述[J]. 机械管理开发, 2022, 37(1): 266-268.
Yu Z B, Zhang Z B, Yin T T, et al. Review of metal 3D printing technology[J]. Mechanical Management and Development, 2022, 37(1): 266-268.

[5] 张学军, 唐思熠, 肇恒跃, 等. 3D 打印技术研究现状和关键技术[J]. 材料工程, 2016, 44(2): 122-128.
Zhang X J, Tang S Y, Zhao H Y, et al. Research status and key technologies of 3D printing[J]. Journal of Materials Engineering, 2016, 44(2): 122-128.

[6] Zhao C, Fezzaa K, Cunningham R W, et al. Real-time monitoring of laser powder bed fusion process using high-speed X-ray imaging and diffraction[J]. Scientific Reports, 2017, 7: 3602.

[7] Gu D D, Meiners W, Wissenbach K, et al. Laser additive manufacturing of metallic components: materials, processes and mechanisms[J]. International Materials Reviews, 2012, 57(3): 133-164.

[8] 吴正凯, 张杰, 吴圣川, 等. 同步辐射 X 射线原位三维成像在金属增材制件缺陷评价中的应用[J]. 无损检测, 2020, 42(7): 46-50.
Wu Z K, Zhang J, Wu S C, et al. Application of *in situ* three-dimensional synchrotron radiation X-ray tomography for defects evaluation of metal additive manufactured components[J]. Nondestructive Testing, 2020, 42(7): 46-50.

[9] An N Y, Shuai S S, Hu T, et al. Application of synchrotron X-ray imaging and diffraction in additive manufacturing: a review[J]. Acta Metallurgica Sinica (English Letters), 2022, 35(1): 25-48.

[10] Ioannidou C, König H H, Semjatov N, et al. *In-situ* synchrotron X-ray analysis of metal additive manufacturing: current state, opportunities and challenges[J]. Materials & Design, 2022, 219: 110790.

[11] Schröder J, Evans A, Mishurova T, et al. Diffraction-based residual stress characterization in laser additive manufacturing of metals[J]. Metals, 2021, 11(11): 1830.

[12] 刘祖平. 同步辐射光源物理引论[M]. 合肥: 中国科学技术大学出版社, 2009: 1-10.
Liu Z P. Introduction to physics of synchrotron radiation source[M]. Hefei: University of Science and Technology of China Press, 2009: 1-10.

[13] 李宜展, 樊潇潇, 曾钢, 等. 同步辐射光源的科技发展及科学影响分析: 以欧洲同步辐射光源为例[J]. 世界科技研究与发展, 2019, 41(1): 16-31.
Li Y Z, Fan X X, Zeng G, et al. The development of science and technology and scientific impact analysis on synchrotron radiation light source: a case study of ESRF[J]. World Sci-Tech R & D, 2019, 41(1): 16-31.

[14] Sun W, Symes D R, Brenner C M, et al. Review of high energy X-ray computed tomography for non-destructive dimensional metrology of large metallic advanced manufactured components[J]. Reports on Progress in Physics, 2022, 85(1): 016102.

[15] 李楠, 王曦, 刘昌奎. 中子衍射技术测量残余应力的研究进展[J]. 失效分析与预防, 2021, 16(2): 148-154.
Li N, Wang X, Liu C K. Research development of residual stress measured by neutron diffraction[J]. Failure Analysis and Prevention, 2021, 16(2): 148-154.

[16] 徐小严, 吕玉廷, 张荻, 等. 中子衍射测量残余应力研究进展[J]. 材料导报, 2015, 29(9): 117-122.
Xu X Y, Lü Y T, Zhang D, et al. Measuring residual stress by neutron diffraction[J]. Materials Review, 2015, 29(9): 117-122.

[17] Rietveld H M. The rietveld method[J]. Physica Scripta, 2014, 89(9): 098002.

[18] 韦杰. 中国散裂中子源简介[J]. 现代物理知识, 2007, 19(6): 22-29.
Wei J. Brief introduction of spallation neutron source in China[J]. Modern Physics, 2007, 19(6): 22-29.

[19] 王沿东, 李润光, 聂志华, 等. 中子/同步辐射衍射表征技术及其在工程材料研究中的应用[J]. 工程科学学报, 2022, 44(4): 676-689.
Wang Y D, Li R G, Nie Z H, et al. A review on the application of neutron and high-energy X-ray diffraction characterization methods in engineering materials[J]. Chinese Journal of Engineering, 2022, 44(4): 676-689.

[20] Sinclair L, Leung C L A, Marussi S, et al. *In situ* radiographic and *ex situ* tomographic analysis of pore interactions during multilayer builds in laser powder bed fusion[J]. Additive Manufacturing, 2020, 36: 101512.

[21] Chen Y H, Clark S J, Leung C L A, et al. *In-situ* synchrotron imaging of keyhole mode multi-layer laser powder bed fusion additive manufacturing[J]. Applied Materials Today, 2020, 20: 100650.

[22] Ahmed F F, Clark S J, Alex Leung C L, et al. Achieving homogeneity in a high-Fe β-Ti alloy laser-printed from blended elemental powders[J]. Materials & Design, 2021, 210: 110072.

[23] Robert O, Knut S, Bernhard H, et al. Synchrotron μ-CT-based morphological characterization of additively manufactured open porous structures[J]. Additive Manufacturing, 2022, 55: 102874.

[24] Leung C L A, Marussi S, Towrie M, et al. Laser-matter interactions in additive manufacturing of stainless steel SS316L and 13-93 bioactive glass revealed by *in situ* X-ray imaging[J]. Additive Manufacturing, 2018, 24: 647-657.

[25] Leung C L A, Marussi S, Atwood R C, et al. *In situ* X-ray imaging of defect and molten pool dynamics in laser additive manufacturing[J]. Nature Communications, 2018, 9: 1355.

[26] Leung C L A, Marussi S, Towrie M, et al. The effect of powder oxidation on defect formation in laser additive manufacturing[J]. Acta Materialia, 2019, 166: 294-305.

[27] Chen Y H, Clark S J, Sinclair L, et al. *In situ* and operando X-ray imaging of directed energy deposition additive manufacturing[EB/OL]. (2020-06-16)[2022-03-04]. https://arxiv.org/abs/2006.09087.

[28] Chen Y H, Clark S J, Collins D M, et al. Correlative synchrotron X-ray imaging and diffraction of directed energy deposition additive manufacturing[J]. Acta Materialia, 2021, 209: 116777.

[29] Chen Y, Clark S, Leung A C L, et al. Melt pool morphology in directed energy deposition additive manufacturing process[J]. IOP Conference Series: Materials Science and Engineering, 2020, 861: 012012.

[30] Parab N D, Zhao C, Cunningham R, et al. Ultrafast X-ray imaging of laser-metal additive manufacturing processes[J]. Journal of Synchrotron Radiation, 2018, 25(5): 1467-1477.

[31] Hojjatzadeh S M H, Guo Q L, Parab N D, et al. *In-situ* characterization of pore formation dynamics in pulsed wave laser powder bed fusion[J]. Materials, 2021, 14(11): 2936.

[32] Gould B, Wolff S, Parab N, et al. *In situ* analysis of laser powder bed fusion using simultaneous high-speed infrared and X-ray imaging[J]. JOM, 2021, 73(1): 201-211.

[33] Simonds B J, Tanner J, Artusio-Glimpse A, et al. The causal relationship between melt pool geometry and energy absorption measured in real time during laser-based manufacturing[J].

Applied Materials Today, 2021, 23: 101049.
[34] Sun T, Tan W D, Chen L Y, et al. *In situ*/operando synchrotron X-ray studies of metal additive manufacturing[J]. MRS Bulletin, 2020, 45(11): 927-933.
[35] Paulson N H, Gould B, Wolff S J, et al. Correlations between thermal history and keyhole porosity in laser powder bed fusion [J]. Additive Manufacturing, 2020, 34: 101213.
[36] Zhao C, Guo Q L, Li X X, et al. Bulk-explosion-induced metal spattering during laser processing [J]. Physical Review X, 2019, 9(2): 021052.
[37] Martin A A, Calta N P, Hammons J A, et al. Ultrafast dynamics of laser-metal interactions in additive manufacturing alloys captured by *in situ* X-ray imaging[J]. Materials Today Advances, 2019, 1: 100002.
[38] Cunningham R, Zhao C, Parab N, et al. Keyhole threshold and morphology in laser melting revealed by ultrahigh-speed X-ray imaging[J]. Science, 2019, 363(6429): 849-852.
[39] Zhao C, Parab N D, Li X X, et al. Critical instability at moving keyhole tip generates porosity in laser melting [J]. Science, 2020, 370(6520): 1080-1086.
[40] Hojjatzadeh S M H, Parab N D, Yan W T, et al. Pore elimination mechanisms during 3D printing of metals [J]. Nature Communications, 2019, 10: 3088.
[41] Hojjatzadeh S M H, Parab N D, Guo Q L, et al. Direct observation of pore formation mechanisms during LPBF additive manufacturing process and high energy density laser welding [J]. International Journal of Machine Tools and Manufacture, 2020, 153: 103555.
[42] Young Z A, Guo Q L, Parab N D, et al. Types of spatter and their features and formation mechanisms in laser powder bed fusion additive manufacturing process[J]. Additive Manufacturing, 2020, 36: 101438.
[43] Li X X, Zhao C, Sun T, et al. Revealing transient powder-gas interaction in laser powder bed fusion process through multi-physics modeling and high-speed synchrotron X-ray imaging [J]. Additive Manufacturing, 2020, 35: 101362.
[44] Derimow N, Schwalbach E J, Benzing J T, et al. *In situ* absorption synchrotron measurements, predictive modeling, microstructural analysis, and scanning probe measurements of laser melted Ti-6Al-4V single tracks for additive manufacturing applications[J]. Journal of Alloys and Compounds, 2022, 900: 163494.
[45] Kantzos C A, Cunningham R W, Tari V, et al. Characterization of metal additive manufacturing surfaces using synchrotron X-ray CT and micromechanical modeling [J]. Computational Mechanics, 2018, 61(5): 575-580.
[46] Gan Z T, Kafka O L, Parab N, et al. Universal scaling laws of keyhole stability and porosity in 3D printing of metals [J]. Nature Communications, 2021, 12: 2379.
[47] Qu M L, Guo Q L, Escano L I, et al. Controlling process instability for defect lean metal additive manufacturing [J]. Nature Communications, 2022, 13: 1079.
[48] Guo Q L, Zhao C, Qu M L, et al. *In-situ* full-field mapping of melt flow dynamics in laser metal additive manufacturing[J]. Additive Manufacturing, 2020, 31: 100939.
[49] Guo Q L, Qu M L, Escano L I, et al. Revealing melt flow instabilities in laser powder bed fusion additive manufacturing of aluminum alloy via *in situ* high-speed X-ray imaging [J]. International Journal of Machine Tools and Manufacture, 2022, 175: 103861.
[50] Guo Q L, Zhao C, Escano L I, et al. Transient dynamics of powder spattering in laser powder bed fusion additive manufacturing process revealed by *in situ* high-speed high-energy X-ray imaging [J]. Acta Materialia, 2018, 151: 169-180.
[51] Guo Q L, Zhao C, Qu M L, et al. *In-situ* characterization and quantification of melt pool variation under constant input energy density in laser powder bed fusion additive manufacturing process[J]. Additive Manufacturing, 2019, 28: 600-609.
[52] Wu Z H, Basu D, Meyer J L L, et al. Study of powder gas entrapment and its effects on porosity in 17-4 PH stainless steel parts fabricated in laser powder bed fusion [J]. JOM, 2021, 73(1): 177-188.
[53] King W E, Barth H D, Castillo V M, et al. Observation of keyhole-mode laser melting in laser powder-bed fusion additive manufacturing[J]. Journal of Materials Processing Technology, 2014, 214(12): 2915-2925.
[54] Chen W Y, Zhang X, Li M M, et al. Laser powder bed fusion of Inconel 718 on 316 stainless steel[J]. Additive Manufacturing, 2020, 36: 101500.
[55] Tang G N, Gould B J, Ngowe A, et al. An updated index including toughness for hot-cracking susceptibility [J]. Metallurgical and Materials Transactions A, 2022, 53(4): 1486-1498.
[56] Jasien C, Saville A, Becker C G, et al. *In situ* X-ray radiography and computational modeling to predict grain morphology in β-titanium during simulated additive manufacturing[J]. Metals, 2022, 12(7): 1217.
[57] Wang H, Gould B, Haddad M, et al. *In situ* X-ray imaging of directed energy deposition of metals: the comparisons of delivery performance between spherical and irregular powders [J]. Journal of Manufacturing Processes, 2022, 79: 11-18.
[58] Wolff S J, Webster S, Parab N D, et al. *In-situ* observations of directed energy deposition additive manufacturing using high-speed X-ray imaging[J]. JOM, 2021, 73(1): 189-200.
[59] Wolff S J, Wang H, Gould B, et al. *In situ* X-ray imaging of pore formation mechanisms and dynamics in laser powder-blown directed energy deposition additive manufacturing [J]. International Journal of Machine Tools and Manufacture, 2021, 166: 103743.
[60] Wang H, Gould B, Moorehead M, et al. *In situ* X-ray and thermal imaging of refractory high entropy alloying during laser directed deposition [J]. Journal of Materials Processing Technology, 2022, 299: 117363.
[61] Pegues J W, Melia M A, Rodriguez M A, et al. *In situ* synchrotron X-ray imaging and mechanical properties characterization of additively manufactured high-entropy alloy composites [J]. Journal of Alloys and Compounds, 2021, 876: 159505.
[62] Wahlmann B, Krohmer E, Breuning C, et al. *In situ* observation of γ' phase transformation dynamics during selective laser melting of CMSX-4 [J]. Advanced Engineering Materials, 2021, 23(11): 2100112.
[63] Krohmer E, Schmeiser F, Wahlmann B, et al. Revealing dynamic processes in laser powder bed fusion with *in situ* X-ray diffraction at PETRA III[J]. Review of Scientific Instruments, 2022, 93(6): 065104.
[64] Schmeiser F, Krohmer E, Schell N, et al. Experimental observation of stress formation during selective laser melting using *in situ* X-ray diffraction [J]. Additive Manufacturing, 2020, 32: 101028.
[65] Uhlmann E, Krohmer E, Schmeiser F, et al. A laser powder bed fusion system for *in situ* X-ray diffraction with high-energy synchrotron radiation [J]. Review of Scientific Instruments, 2020, 91(7): 075104.
[66] Schmeiser F, Krohmer E, Schell N, et al. Internal stress evolution and subsurface phase transformation in titanium parts manufactured by laser powder bed fusion: an *in situ* X-ray diffraction study[J]. Advanced Engineering Materials, 2021, 23(11): 2001502.
[67] Epp J, Dong J, Meyer H, et al. Analysis of cyclic phase transformations during additive manufacturing of hardenable tool steel by *in situ* X-ray diffraction experiments[J]. Scripta Materialia, 2020, 177: 27-31.
[68] Calta N P, Wang J, Kiss A M, et al. An instrument for *in situ*

time-resolved X-ray imaging and diffraction of laser powder bed fusion additive manufacturing processes[J]. Review of Scientific Instruments, 2018, 89(5): 055101.

[69] Thampy V, Fong A Y, Calta N P, et al. Subsurface cooling rates and microstructural response during laser based metal additive manufacturing[J]. Scientific Reports, 2020, 10: 1981.

[70] Martin A A, Calta N P, Khairallah S A, et al. Dynamics of pore formation during laser powder bed fusion additive manufacturing[J]. Nature Communications, 2019, 10: 1987.

[71] Calta N P, Martin A A, Hammons J A, et al. Pressure dependence of the laser-metal interaction under laser powder bed fusion conditions probed by *in situ* X-ray imaging[J]. Additive Manufacturing, 2020, 32: 101084.

[72] Kiss A M, Fong A Y, Calta N P, et al. Laser-induced keyhole defect dynamics during metal additive manufacturing[J]. Advanced Engineering Materials, 2019, 21(10): 1970031.

[73] Martin A A, Wang J, DePond P J, et al. A laser powder bed fusion system for operando synchrotron X-ray imaging and correlative diagnostic experiments at the Stanford Synchrotron Radiation Lightsource[J]. The Review of Scientific Instruments, 2022, 93(4): 043702.

[74] Calta N P, Thampy V, Lee D R C, et al. Cooling dynamics of two titanium alloys during laser powder bed fusion probed with *in situ* X-ray imaging and diffraction[J]. Materials & Design, 2020, 195: 108987.

[75] Hocine S, van Petegem S, Frommherz U, et al. A miniaturized selective laser melting device for operando X-ray diffraction studies[J]. Additive Manufacturing, 2020, 34: 101194.

[76] Hocine S, van Swygenhoven H, van Petegem S, et al. Operando X-ray diffraction during laser 3D printing[J]. Materials Today, 2020, 34: 30-40.

[77] Ghasemi-Tabasi H E, de Formanoir C, van Petegem S, et al. Direct observation of crack formation mechanisms with operando laser powder bed fusion X-ray imaging[J]. Additive Manufacturing, 2022, 51: 102619.

[78] Glerum J A, Hocine S, Chang C S T, et al. Operando X-ray diffraction study of thermal and phase evolution during laser powder bed fusion of Al-Sc-Zr elemental powder blends[J]. Additive Manufacturing, 2022, 55: 102806.

[79] Dass A, Gabourel A, Pagan D, et al. Laser based directed energy deposition system for operando synchrotron X-ray experiments[J]. The Review of Scientific Instruments, 2022, 93(7): 075106.

[80] Zhang X X, Lutz A, Andrä H, et al. Strain hardening behavior of additively manufactured and annealed AlSi3.5Mg2.5 alloy[J]. Journal of Alloys and Compounds, 2022, 898: 162890.

[81] An K, Yuan L, Dial L, et al. Neutron residual stress measurement and numerical modeling in a curved thin-walled structure by laser powder bed fusion additive manufacturing[J]. Materials & Design, 2017, 135: 122-132.

[82] Sofras C, Čapek J, Arabi-Hashemi A, et al. Tailored deformation behavior of 304L stainless steel through control of the crystallographic texture with laser-powder bed fusion[J]. Materials & Design, 2022, 219: 110789.

[83] Pant P, Salvemini F, Proper S, et al. A study of the influence of novel scan strategies on residual stress and microstructure of L-shaped LPBF IN718 samples[J]. Materials & Design, 2022, 214: 110386.

[84] Tang L, Magdysyuk O, Jiang F Q, et al. Mechanical performance and deformation mechanisms at cryogenic temperatures of 316L stainless steel processed by laser powder bed fusion: *in situ* neutron diffraction[J]. Scripta Materialia, 2022, 218: 114806.

[85] Masoomi M, Shamsaei N, Winholtz R A, et al. Residual stress measurements via neutron diffraction of additive manufactured stainless steel 17-4 PH[J]. Data in Brief, 2017, 13: 408-414.

[86] Reid M, Sercombe T, Paradowska A, et al. Residual stresses in selective laser melted components of different geometries[J]. Materials Research Proceedings, 2017, 2: 383-388.

[87] Nadammal N, Cabeza S, Mishurova T, et al. Effect of hatch length on the development of microstructure, texture and residual stresses in selective laser melted superalloy Inconel 718[J]. Materials & Design, 2017, 134: 139-150.

[88] Luzin V, Kirstein O, Zahiri S H, et al. Residual stress buildup in Ti components produced by cold spray additive manufacturing (CSAM)[J]. Journal of Thermal Spray Technology, 2020, 29(6): 1498-1507.

[89] Shen C, Ma Y, Reid M, et al. Neutron diffraction residual stress determinations in titanium aluminide component fabricated using the twin wire-arc additive manufacturing[J]. Journal of Manufacturing Processes, 2022, 74: 141-150.

[90] Hasani N, Ghoncheh M H, Kindermann R M, et al. Dislocations mobility in superalloy-steel hybrid components produced using wire arc additive manufacturing[J]. Materials & Design, 2022, 220: 110899.

[91] Honnige J R, Williams S, Roy M J, et al. Residual stress characterization and control in the additive manufacture of large scale metal structures[J]. Materials Research Proceedings, 2017, 2: 455-460.

[92] Kim Y S, Chae H, Woo W, et al. Multiple deformation scheme in direct energy deposited CoCrNi medium entropy alloy at 210 K[J]. Materials Science and Engineering: A, 2021, 828: 142059.

[93] Wang Z Q, Stoica A D, Ma D, et al. Diffraction and single-crystal elastic constants of Inconel 625 at room and elevated temperatures determined by neutron diffraction[J]. Materials Science and Engineering: A, 2016, 674: 406-412.

[94] Wang Z Q, Denlinger E, Michaleris P, et al. Residual stress mapping in Inconel 625 fabricated through additive manufacturing: method for neutron diffraction measurements to validate thermomechanical model predictions[J]. Materials & Design, 2017, 113: 169-177.

[95] Ma D, Stoica A D, Wang Z Q, et al. Crystallographic texture in an additively manufactured nickel-base superalloy[J]. Materials Science and Engineering: A, 2017, 684: 47-53.

[96] Kirkwood H J, Zhang S Y, Tremsin A S, et al. High resolution imaging and analysis of residual elastic strain in an additively manufactured turbine blade[J]. International Journal of Nanotechnology, 2016, 14(1/2/3/4/5/6): 166-178.

[97] Cakmak E, Kirka M M, Watkins T R, et al. Microstructural and micromechanical characterization of IN718 theta shaped specimens built with electron beam melting[J]. Acta Materialia, 2016, 108: 161-175.

[98] Xie Q, Song G, Gorti S, et al. Applying neutron transmission physics and 3D statistical full-field model to understand 2D Bragg-edge imaging[J]. Journal of Applied Physics, 2018, 123(7): 074901.

[99] Hrabe N, Gnäupel-Herold T, Quinn T. Fatigue properties of a titanium alloy (Ti-6Al-4V) fabricated via electron beam melting (EBM): effects of internal defects and residual stress[J]. International Journal of Fatigue, 2017, 94: 202-210.

[100] Cao J, Gharghouri M A, Nash P. Finite-element analysis and experimental validation of thermal residual stress and distortion in electron beam additive manufactured Ti-6Al-4V build plates[J]. Journal of Materials Processing Technology, 2016, 237: 409-419.

[101] Clausen B, Brown D W, Carpenter J S, et al. Deformation behavior of additively manufactured GP1 stainless steel[J]. Materials Science and Engineering: A, 2017, 696: 331-340.

[102] Ghasri-Khouzani M, Peng H, Rogge R, et al. Experimental measurement of residual stress and distortion in additively manufactured stainless steel components with various dimensions[J]. Materials Science and Engineering: A, 2017,

707: 689-700.
[103] Zhang X, Yocom C J, Mao B, et al. Microstructure evolution during selective laser melting of metallic materials: a review [J]. Journal of Laser Applications, 2019, 31(3): 031201.
[104] Jakumeit J, Zheng G Y, Laqua R, et al. Modelling the complex evaporated gas flow and its impact on particle spattering during laser powder bed fusion[J]. Additive Manufacturing, 2021, 47: 102332.
[105] Wei H L, Mukherjee T, Zhang W, et al. Mechanistic models for additive manufacturing of metallic components[J]. Progress in Materials Science, 2021, 116: 100703.
[106] Bobel A, Hector L G, Jr, Chelladurai I, et al. *In situ* synchrotron X-ray imaging of 4140 steel laser powder bed fusion[J]. Materialia, 2019, 6: 100306.
[107] Krakhmalev P, Fredriksson G, Yadroitsava I, et al. Deformation behavior and microstructure of Ti6Al4V manufactured by SLM [J]. Physics Procedia, 2016, 83: 778-788.
[108] Carlton H D, Haboub A, Gallegos G F, et al. Damage evolution and failure mechanisms in additively manufactured stainless steel [J]. Materials Science and Engineering: A, 2016, 651: 406-414.
[109] Tammas-Williams S, Zhao H, Léonard F, et al. XCT analysis of the influence of melt strategies on defect population in Ti-6Al-4V components manufactured by selective electron beam melting[J]. Materials Characterization, 2015, 102: 47-61.
[110] Tammas-Williams S, Withers P J, Todd I, et al. The effectiveness of hot isostatic pressing for closing porosity in titanium parts manufactured by selective electron beam melting [J]. Metallurgical and Materials Transactions A, 2016, 47(5): 1939-1946.
[111] Tammas-Williams S, Withers P J, Todd I, et al. Porosity regrowth during heat treatment of hot isostatically pressed additively manufactured titanium components [J]. Scripta Materialia, 2016, 122: 72-76.
[112] Wu S C, Hu Y N, Song Z, et al. Fatigue behaviors of laser hybrid welded AA7020 due to defects via synchrotron X-ray microtomography [J]. Fatigue & Fracture of Engineering Materials & Structures, 2019, 42(10): 2232-2246.
[113] Bao J G, Wu S C, Withers P J, et al. Defect evolution during high temperature tension-tension fatigue of SLM AlSi10Mg alloy by synchrotron tomography [J]. Materials Science and Engineering: A, 2020, 792: 139809.
[114] Hu D Y, Pan J C, Mao J X, et al. Mechanical behavior prediction of additively manufactured components based on defect evolution observation by synchrotron radiation X-ray tomography[J]. Materials & Design, 2021, 198: 109353.
[115] Qian W J, Wu S C, Wu Z K, et al. *In situ* X-ray imaging of fatigue crack growth from multiple defects in additively manufactured AlSi10Mg alloy [J]. International Journal of Fatigue, 2022, 155: 106616.
[116] Mercelis P, Kruth J P. Residual stresses in selective laser sintering and selective laser melting [J]. Rapid Prototyping Journal, 2006, 12(5): 254-265.
[117] Serrano-Munoz I, Fritsch T, Mishurova T, et al. On the interplay of microstructure and residual stress in LPBF IN718 [J]. Journal of Materials Science, 2021, 56(9): 5845-5867.
[118] Zhu B, Leung N, Kockelmann W, et al. Revealing the residual stress distribution in laser welded Eurofer97 steel by neutron diffraction and Bragg edge imaging [J]. Journal of Materials Science & Technology, 2022, 114: 249-260.
[119] Matsushima M, Jin X J, Shiota Y, et al. Neutron diffraction measurement of thermal residual stresses caused by solution treatment for a SUS304 stainless steel mechanical part [M]// Sung J H, Lee C G, You Y Z, et al. Solid state phenomena. Stafa: Trans Tech Publications Ltd., 2006: 425-430.
[120] Jiang W C, Wan Y, Tu S T, et al. Determination of the through-thickness residual stress in thick duplex stainless steel welded plate by wavelength-dependent neutron diffraction method [J]. International Journal of Pressure Vessels and Piping, 2022, 196: 104603.
[121] Aminforoughi B, Degener S, Richter J, et al. A novel approach to robustly determine residual stress in additively manufactured microstructures using synchrotron radiation [J]. Advanced Engineering Materials, 2021, 23(11): 2100184.
[122] Xu W, Brandt M, Sun S, et al. Additive manufacturing of strong and ductile Ti-6Al-4V by selective laser melting via *in situ* martensite decomposition [J]. Acta Materialia, 2015, 85: 74-84.
[123] Rangaswamy P, Holden T M, Rogge R B, et al. Residual stresses in components formed by the laserengineered net shaping (LENS®) process[J]. The Journal of Strain Analysis for Engineering Design, 2003, 38(6): 519-527.
[124] Shen J J, Zeng Z, Nematollahi M, et al. *In-situ* synchrotron X-ray diffraction analysis of the elastic behaviour of martensite and H-phase in a NiTiHf high temperature shape memory alloy fabricated by laser powder bed fusion[J]. Additive Manufacturing Letters, 2021, 1: 100003.
[125] Wahlmann B, Galgon F, Stark A, et al. Growth and coarsening kinetics of gamma prime precipitates in CMSX-4 under simulated additive manufacturing conditions [J]. Acta Materialia, 2019, 180: 84-96.
[126] Beese A M, Wang Z Q, Stoica A D, et al. Absence of dynamic strain aging in an additively manufactured nickel-base superalloy[J]. Nature Communications, 2018, 9: 2083.
[127] Mori M, Yamanaka K, Onuki Y, et al. Analysis of hierarchical microstructural evolution in electron beam powder bed fusion Ti-6Al-4V alloys via time-of-flight neutron diffraction[J]. Additive Manufacturing Letters, 2022, 3: 100053.
[128] Xie Y, Vogel S C, Harp J M, et al. Microstructure evolution of U-Zr system in a thermal cycling neutron diffraction experiment: extruded U-10Zr (wt. %)[J]. Journal of Nuclear Materials, 2021, 544: 152665.
[129] Miao Y B, Mo K, Park J S, et al. *In situ* synchrotron tensile investigations on ultrasonic additive manufactured (UAM) zirconium [J]. Journal of Nuclear Materials, 2022, 568: 153843.
[130] Prasad K, Horita Y, Ito A, et al. *In situ* synchrotron diffraction study of a crack-free additively manufactured Ni base superalloy[J]. Scripta Materialia, 2021, 200: 113896.
[131] 高钰璧, 丁雨田, 李海峰, 等. 变形速率对 GH3625 合金弹-塑性变形行为的影响[J]. 金属学报, 2022, 58(5): 695-708.
Gao Y B, Ding Y T, Li H F, et al. Effect of deformation rate on the elastic-plastic deformation behavior of GH3625 alloy[J]. Acta Metallurgica Sinica, 2022, 58(5): 695-708.
[132] Ashby M F. The deformation of plastically non-homogeneous materials [J]. The Philosophical Magazine: A Journal of Theoretical Experimental and Applied Physics, 1970, 21(170): 399-424.
[133] Laquai R, Müller B R, Schneider J A, et al. Using SXRR to probe the nature of discontinuities in SLM additive manufactured Inconel 718 specimens [J]. Metallurgical and Materials Transactions A, 2020, 51(8): 4146-4157.
[134] Li X S, Zweiacker K, Grolimund D, et al. *In situ* and *ex situ* characterization of the microstructure formation in Ni-Cr-Si alloys during rapid solidification: toward alloy design for laser additive manufacturing[J]. Materials, 2020, 13(9): 2192.
[135] 魏志勇, 臧黎慧, 范我, 等. 利用中子散射研究生物材料[J]. 核技术, 2006, 29(9): 713-720.
Wei Z Y, Zang L H, Fan W, et al. Study of biological materials by neutron scattering[J]. Nuclear Techniques, 2006, 29(9): 713-720.
[136] Fitzpatrick M E, Lodini A. Book review: analysis of residual stress by diffraction using neutron and synchrotron radiation [J]. Measurement Science and Technology, 2003, 14(9): 1739-1740.

Application of Synchrotron Radiation and Neutron Diffraction Technologies in Additive Manufacturing

Deng Hongwen[1,2,4], Zhang yi[2,3,4], Quan Aodong[1,2,4], Wang Yudai[2,3,4], Tang Haibo[2,3,4], Cheng Xu[2,3,4*]

[1] *School of Materials Science and Engineering, Beihang University, Beijing* 100191, *China*;

[2] *National Engineering Laboratory of Additive Manufacturing for Large Metallic Components and Engineering Research Center, Beihang University, Beijing* 100191, *China*;

[3] *Research Institute for Frontier Science, Beihang University, Beijing* 100191, *China*;

[4] *Beijing Engineering Technological Research Center on Laser Direct Manufacturing for Large Critical Metallic Component, Beijing* 100191, *China*

Abstract

Significance Metal additive manufacturing (MAM) processes can directly produce fully dense near net shape components, which are widely used in aerospace, medical, and defense applications. Due to its unique fabrication benefits, additive manufacturing has become one of the fastest-growing and most-active research directions worldwide. However, MAM is carried out under extreme thermodynamic conditions that involve metal melting and solidification, interactions among different elements, and generation of thermal stresses. Hence, various internal defects, such as lack of fusion porosity, pores, cracks, and internal stresses, will inevitably be generated during the MAM process. Normally, defects and residual stresses will significantly affect the quality and mechanical properties of the MAMed components. To eliminate the defects and control the residual stresses, researchers have been focusing on the kinetic behavior of the molten pool, formation mechanism of defects and unstable solid-state phase transformations, and the evolution of the residual stresses. It is wildly recognized that *in situ* characterization of the defect formation mechanisms in the molten pool and monitoring of the residual stress changes during the MAM process is very challenging. Because the traditional measurement techniques, such as X-ray detection, X-ray diffraction, and ultrasonic detection, can only analyze defects and residual stresses after the components have been manufactured, it is necessary to find a technique capable of performing *in situ* analysis during the MAM process.

The rapidly developing synchrotron radiation and neutron diffraction-based characterization technologies have proven to be some of the most effective methods for *in situ* analysis of defect formation mechanisms, crack initiation, phase transformation, and stress evolution during the AM process. This paper reviews the principles of synchrotron radiation and neutron diffraction technologies and their advantages and practical applications in AM, and summarizes the recent progress and future prospects of their applications in AM.

Progress Over the past decade, with the rapid development of characterization techniques based on synchrotron radiation and neutron diffraction, a large volume of research has been carried out to investigate the formation mechanisms and distribution of internal stresses during the AM process (Tables 1 and 2). The synchrotron radiation-based characterization methods can broadly be divided into the following three different types: synchrotron X-ray imaging, synchrotron X-ray diffraction, and synchrotron computed tomography. The synchrotron X-ray imaging can characterize *in situ* the formation process of internal three-dimensional defects in materials and analyze *in situ* the molten pool dynamics. The synchrotron X-ray diffraction can be used to analyze the internal stress states and phase transformation processes in materials, and works with the tensile test to dynamically analyze *in situ* the internal dislocation density of parts. The synchrotron computed tomography can reconstruct three-dimensional models of additively manufactured components to analyze surface defects, and can assess the impact of internal defects during the service process of components using *in situ* mechanical tests. The neutron diffraction technologies can be divided into non-*in-situ* neutron diffraction, *in situ* neuron diffraction, and electrically neutral nuclear scattering techniques. In addition to examining the macroscopic residual stresses in additive components, the characterization based on the neutron diffraction technologies can also measure the metal texture, crystal lattice parameter changes, strain, grain size, density of dislocations, and other parameters. It can also detect the concentration and the location of light elements, such as hydrogen and lithium, in the crystalline structure. Using the synchrotron X-ray imaging, Qu of the University of Wisconsin-Madison, has discovered that nanoparticles can be adopted to eliminate all types of large spatters by simultaneously stabilizing molten pool fluctuations and controlling liquid droplet coalescence. They have also demonstrated that the control of laser powder bed interaction instabilities by TiC nanoparticles is feasible, which has led to the elimination of large spatters and printing

of lean-defect samples with good consistency and enhanced properties (Figure 2). Beese of the Pennsylvania State University and Oak Ridge National Laboratory performed *in situ* neutron diffraction studies of lattice strain evolution and offered a new perspective on the understanding of dislocation-solute interactions and their impact on work-hardening behavior in high-temperature alloys. These observations can pave the way for a fundamental understanding of the abnormal increase in strength at elevated temperatures commonly observed in a wide range of high-temperature structural alloys and may have important implications for tailoring thermomechanical properties using microstructure control in MAM.

Conclusions and Prospects Although the characterization techniques based on synchrotron radiation and neutron diffraction have been widely used in the AM process, further development is still needed to expand their applications in AM along the following directions. *In situ* detection techniques still need improvements, and the temperature field, velocity field, cooling rate, and solidification parameters must be considered in real-time models to reduce the internal defects and improve the quality of additively manufactured components. In addition, *in situ* inspection of the deposition processes should combine high-resolution and ultrafast synchrotron X-ray imaging, high-speed light photography, and infrared thermometry to develop *in situ* AM characterization techniques with higher resolution and contrast sensitivity. Furthermore, molten pool dynamics models should be established, which can then guide the design and optimization of AM process parameters. Meanwhile, taking the advantage of the synchrotron radiation and neutron-based X-ray diffraction techniques, the internal stress distribution and microstructure evolution during metal forming and servicing processes can be analyzed. Moreover, the advantages of adopting the synchrotron radiation and neutron-based techniques for measuring the three-dimensional stress field at the crack tip can help to establish the elastoplastic nonlinear micromechanical models of additively manufactured components, which can be used to analyze the fatigue and fractures caused by the multiscale stress field variations.

Key words laser technique; additive manufacturing; synchrotron radiation; neutron diffraction; material characterization